SAND2020-6551R

I Advanced Combustion Systems

I.1 ACE001: Heavy-Duty Diesel Combustion (Sandia National Laboratories)

Mark PB Musculus, Principal Investigator
Sandia National Laboratories
PO Box 969, MS 9053
Livermore, CA 94551-0969
E-mail: mpmuscu@sandia.gov

Gurpreet Singh, DOE Program Manager
U.S. Department of Energy
E-mail: gurpreet.singh@ee.doe.gov

Start Date: October 1, 2018 End Date: September 30, 2019
Project Funding (FY18): $880k DOE share: $880k Non-DOE share: $0

Project Introduction

Regulatory drivers and market demands for lower pollutant emissions, lower carbon dioxide emissions, and lower fuel consumption motivate the development of cleaner and more fuel-efficient engine operating strategies. Most current production engines use a combination of both in-cylinder and exhaust emissions-control strategies to achieve these goals. The emissions and efficiency performance of in-cylinder strategies depend strongly on flow and mixing processes associated with fuel injection and heat losses.

Low heat transfer (HT) is desirable to increase engine thermal efficiency and/or to increase exhaust temperatures to improve performance of turbocharging, exhaust emissions controls, and waste heat recovery. A large contributor to the higher thermal efficiency of advanced combustion modes is often a reduction in heat transfer. For instance, reactivity-controlled compression-ignition (RCCI) has achieved indicated thermal efficiencies as high as 59% relative to 47% for conventional diesel, with HT losses reduced from 16% down to 11% [1]. Even though the heat transfer was responsible for much of the improvement in efficiency, the reduction was largely serendipitous, without direct design intention to reduce heat transfer, which is generally difficult to achieve. Indeed, this year in a new report of efforts to achieve 21st Century Truck Partnership goals for 50% or higher brake thermal efficiency, engineers from Cummins noted that HT is responsible for over 50% of the gap between theoretical and realized engine efficiency, making it the "the largest area of opportunity, but also arguably the most difficult to impact" [2]. Different combustion modes have different spatio-temporal evolution of in-cylinder combustion/flows that affect HT, so to design combustion to minimize HT, it is important to understand how in-cylinder processes of different combustion modes affect HT.

Objectives

This project includes diesel combustion research at Sandia National Laboratories (SNL) and combustion nd flow modeling and simulation by Wisconsin Engine Research Consultants (WERC).

Overall Objectives

- Develop fundamental understanding of how in-cylinder controls can improve efficiency and reduce pollutant emissions of both conventional diesel and advanced low-temperature combustion (LTC)
- Quantify the effects of fuel injection, mixing, and combustion processes on thermodynamic losses and pollutant emission formation
- Improve computer modeling capabilities to accurately simulate these processes

Fiscal Year 2019 Objectives

- Develop and apply diagnostics to quantify combustion-mode effects on heat transfer and efficiency
- Use simulation predictions to guide and complement multiple injection experiments
- Determine how mixing and jet interactions are affected by in-cylinder flows, the decay of spray-generated turbulence, large-scale structures, and/or entrainment-wave-effects on the bulk-jet during the injection dwell

Approach

This project uses an optically-accessible, heavy-duty, direct-injection diesel engine (Figure 1). For the heat transfer measurements, 13 fast-acting (2.5 microsecond response time) surface thermocouples are installed into a round puck that is mounted into the cylinder wall, as shown in the photograph in the lower-right of Figure 1. The surface heat flux (HF) during combustion in the engine is derived from the transient temperature response of the cylinder-wall thermocouples. The piston crown has a cut-out in line with the thermocouples so that the the thermocouples are directly are exposed to impinging diesel jets and combustion. As shown in Figure 1, two fueling options are available, either by gasoline direct injection (GDI) using a Bosch side-injector mounted in the cylinder wall, or by a centrally mounted Delphi DFI-1.5 common-rail diesel injector. The choice of injector(s) for the experiments depends on the combustion mode, as described in the results section.

For the results presented here, a window in place of one of the exhaust valves in the cylinder head provides imaging access to the squish region above the piston, as well as to a small portion of the piston bowl, in line with one of the diesel jet trajectories. A high-speed intensified complementary metal oxide semiconductor (ICMOS) camera equipped with a 310-nm bandpass filter images chemiluminescence emission from excited state hydroxyl radicals (OH*), which are produced during combustion in relatively hot regions. Hence, the OH* imaging combined with thermocouple measurements shows the interaction between in-cylinder combustion and HT losses.

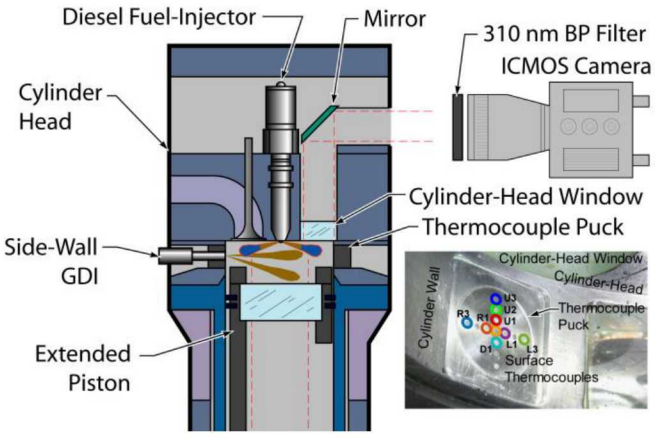

Figure 1. Schematic showing the top half of the optical engine. Fueling options are a side-wall mounted GDI and a centrally located diesel fuel injector. The annotated photograph on the bottom-right shows a round puck with surface thermocouples that is mounted in the cylinder wall. The camera postion provides for imaging through the cylinder head window.

Results

Figure 2 shows results from a homogeneous-charge compression-ignition (HCCI) type of operating condition, using a premixture of gasoline primary reference fuels (PRF) n-heptane and iso-octane at a load of 4.8 bar gross indicated mean effective pressure (IMEPg). The GDI and diesel injectors were actuated near the beginning of the intake stroke to deliver iso-octane and n-heptane, respectively, in quantities with iso-octane at 57% of the total mixture (PRF57). With such early injection, the fuels were relatively homogeneous at ignition.

In Figure 2, four key OH* chemiluminescence images at different crank angle degree (CAD) positions from one of the cycles show the progression of combustion. The measured heat flux for each of the thermocouples, as well as the apparent heat release rate (AHRR), are plotted above the images. In each of the images, the approximate location of key thermocouples in each image is indicated by color-coded and labeled circles according to Figure 1. From the perspective of the camera, thermocouples D1, T0, and U1-U3 are nearly along the camera line of sight so that they appear close together in the image.

In the plot at the top of Figure 2, the HF generally increases slightly after low-temperature heat-release (LTHR) near 346 CAD, though this is not visible in the images because no detectable OH* chemiluminescence is emitted during LTHR. Weak OH* chemiluminescence first appears at 366 CAD, near the peak AHRR. The OH* chemiluminescence quickly brightens at 367 CAD as HF of all thermocouples starts to increase, all at nearly the same time. OH* chemiluminescence quickly disappears after 368 CAD, near end of the heat release, while the HF continues after combustion while hot gases are near the wall, such that the HF spikes are not as narrow nor in phase with the AHRR.

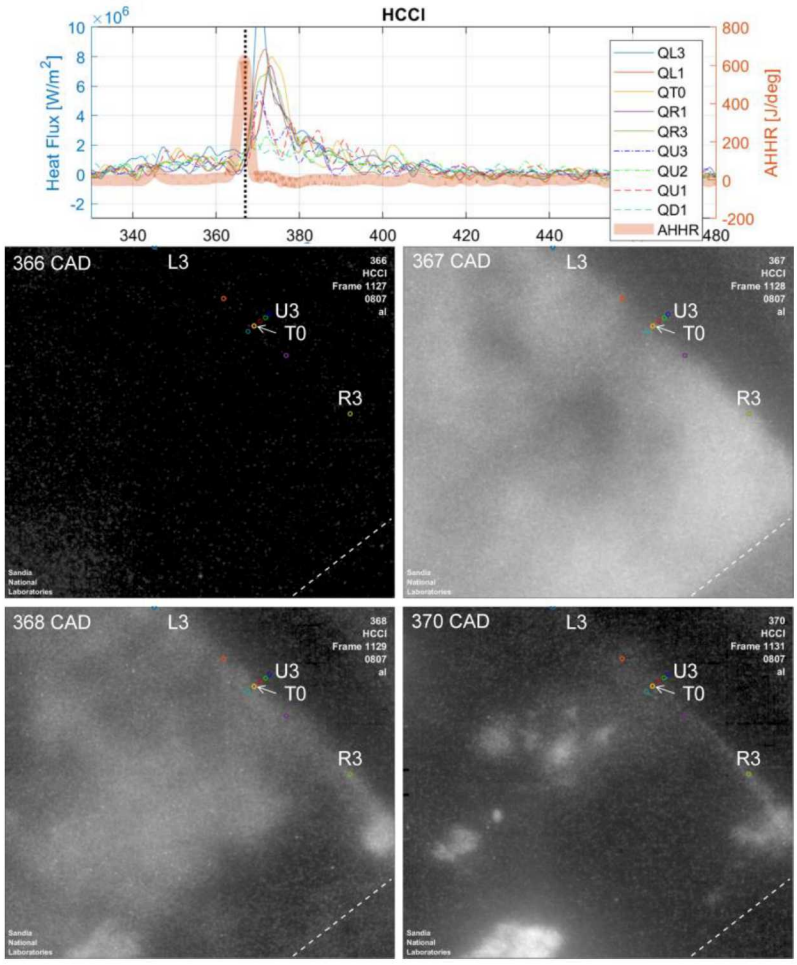

Figure 2. AHRR and thermocouple HF measurements (top) and key OH* chemiluminescence images from one cycle of HCCI-type combustion. See Figure 1 for physical locations of thermocouples in the images indicated by labels and color-coded circles.

While the HF of all thermocouples can be characterized as increasing sharply at the onset of rapid combustion for the premixed conditions of Figure 2, the characteristics are different for other combustion modes. Figure 3 shows corresponding HF, AHRR, and key OH* chemiluminescence images for a conventional diesel combustion (CDC) condition, for which the diesel injector delivers n-heptane starting at 350 CAD and at a

load of 4.3 bar IMEPg. The diesel injector is mounted in the cylinder head such that the trajectory of one of the jets is aligned with thermocouples D1, T0, and U1-U3 from the perspective of the camera. In the images in Figure 3, the luminosity recorded in the images includes not only OH* chemiluminescence, but also some soot natural luminosity. Also, the energizing of the injector solenoid interferes with the HF measurements, appearing as a downward and then upward spike from 347 to 353 CAD.

For this operating condition, the ignition delay is relatively short, so a hot diffusion flame is established before the jet impinges on wall where the thermocouples are located. Starting shortly after the start of combustion and after the injector solenoid energizing interference has ceased, the HF has increased from 360 CAD to about 366 CAD, where it then increases more sharply. The OH chemiluminescence images show that jet impingement on the wall occurs near 363 CAD, however. The low-level HF ahead of jet impingement (as indicated by OH* images) could be due in part to the pressure rise associated with combustion, radiative heat transfer, or compression of the boundary layer ahead of the jet. After impingement, the thermocouples in-line with the jet axis increase first, followed by thermocouples on either side of the jet, matching the spatial progression observed in the OH* chemiluminescence images as the jet impinges and flattens on the wall. However, there is a 3-degree crank-angle delay from impingement observed in the OH* chemiluminescence images to the rapid increase in heat flux. This also may be due to compression of the boundary layer ahead of the jet, or potentially to soot deposits for CDC conditions that may insulate the thermocouples for a short time.

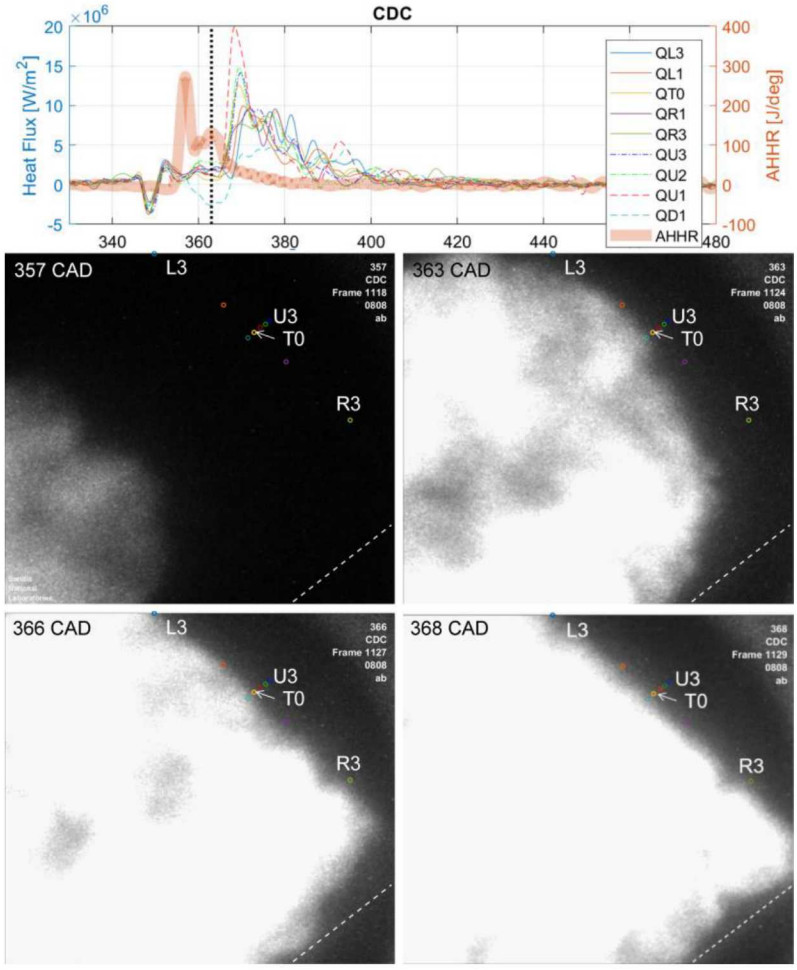

Figure 3. AHRR and thermocouple HF measurements (top) and key OH* chemiluminescence images from one cycle of conventional diesel combustion. See Figure 1 for physical locations of thermocouples in the images indicated by labels and color-coded circles.

A third operating condition, partially premixed compression-ignition (PPCI), is shown in Figure 4. This operating condition also uses n-heptane delivered by the diesel injector, but with an earlier start of injection at 335 CAD at a load of 4.0 bar IMEPg and with nitrogen dilution of the intake oxygen to 12.6% to simulate LTC conditions using high exhaust gas recirculation (EGR). For this condition, the OH* chemiluminescence images show that ignition starts near the wall and quickly proceeds through the rest of the impinged jet, resulting in a narrow AHRR spike at the top of Figure 4. Similar to the CDC condition, low-level HF precedes hot ignition, but in this case, it is more likely due to direct jet impingement on the wall, though some boundary layer compression may also contribute.

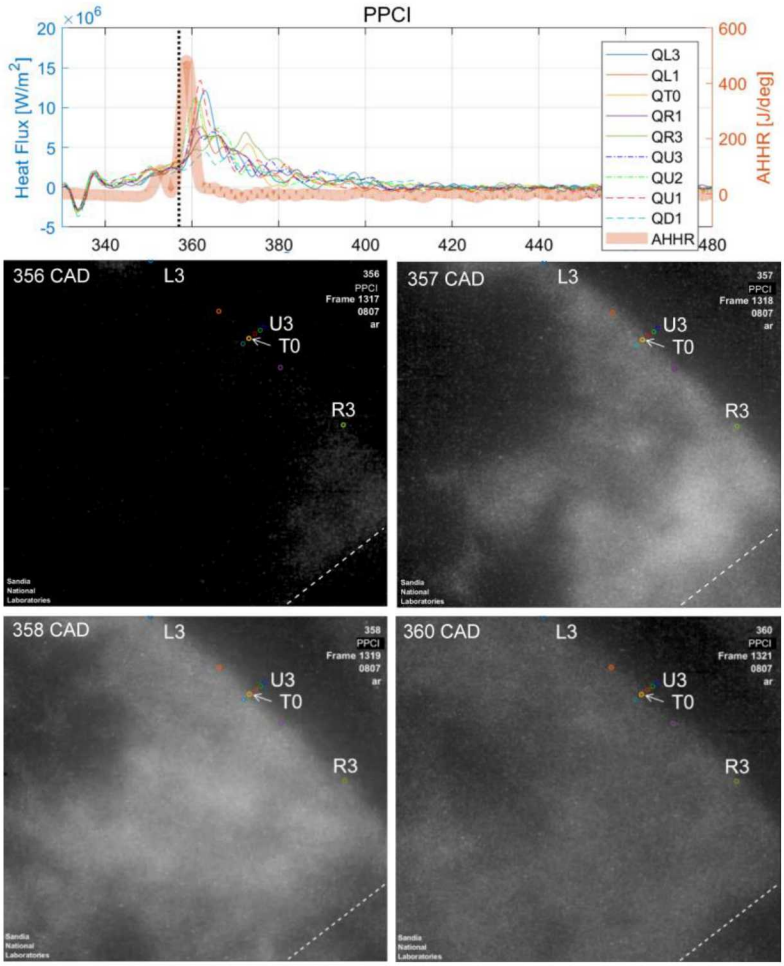

Figure 4. AHRR and thermocouple HF measurements (top) and key OH* chemiluminescence images from one cycle of partially premixed compression ignition. See Figure 1 for physical locations of thermocouples in the images indicated by labels and color-coded circles.

To explore the possible contribution of boundary layer compression to increased HF, simple scaling arguments are invoked. Figure 5 shows a comparison of fired and motored HF for the CDC condition, with the shaded area indicating the difference in HF before jet impingement on the wall. Also shown in Figure 5 are two different scalings of the motored heat flux according to two limiting scenarios, either one-dimensional scaling of the boundary layer thickness according to the penetration distance of the jet, or isotropic scaling according to the volume of the penetrating jet. The effects of real three-dimensional fluid mechanics ahead of the jet that compress the boundary layer are expected to lie between these two extremes. Indeed, the measured HF lies between these two limits, suggesting that boundary layer compression may play in important role in local heat transfer losses for operating conditions with jet impingement. However, other measurements in the literature in a constant-volume chamber did not observe a HF increase ahead of jet impingement [3], so this hypothesis

needs to be revisited more carefully under fully non-reacting conditions where complications from combustion are not present.

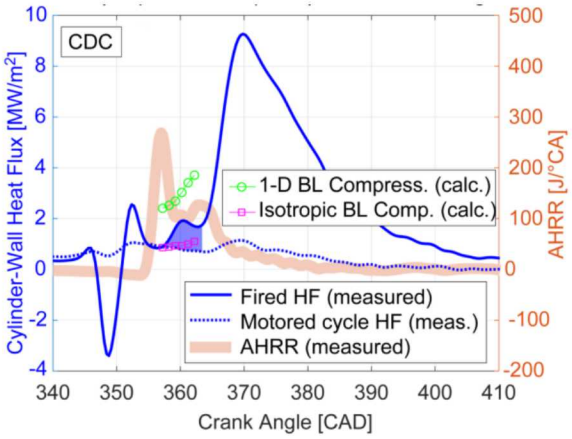

Figure 5. Fired and motored thermocouple HF measurements and AHRR for conventional diesel combustion, with shaded area indicating the differnce between fired and motored HF ahead of jet impingement. Predictions from two simple scaling models are also included.

Finally, in addition to the work on wall HF, simulation activities continued to develop insight into the interactions between multiple injections. Figure 6 shows cross sections of fuel, carbon monoxide (CO), and OH in a split-injection diesel jet as predicted by the simulations. The contributions to each of these quantities from the fuel of the two injections is separated in the plots. At the start of second-stage ignition, the simulations show that the second injection has mixed with first injection residual jet to greatly increase local fuel concentration – the red color in the top fuel image, indicating high fuel concentration, is almost entirely from the second injection. Even so, products from first-stage ignition, such as CO, are primarily from first-injection fuel, again shown by the red color in the CO cross-sections. Importantly, the simulations therefore predict that the second injection fuel is intimately mixed with first-stage ignition products of the first injection as the second-stage ignition commences. Later, after ignition, the OH cross-sections show that second-stage ignition products, such as OH, are primarily from the first-injection fuel. Even so, the simulations with a single injection show that the first injection would not ignite without the second injection. These simulation predictions provide guidance for planning what key measurements to include in fundamental experiments on mixing between injections and effects on ignition.

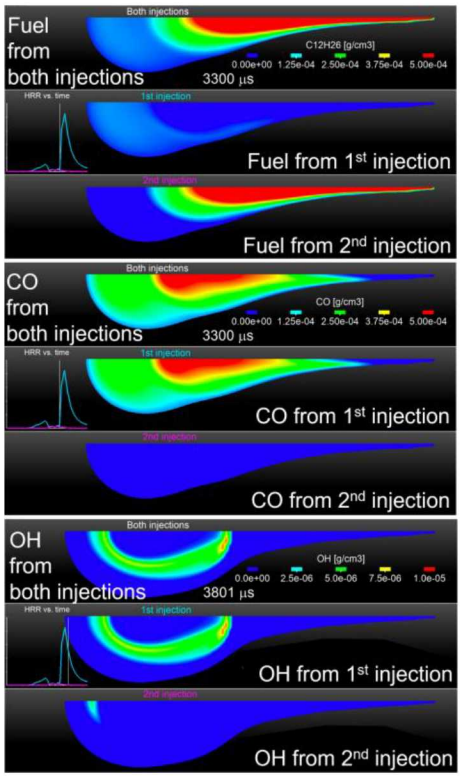

Figure 6. Cross-sections of simulation-predicted fuel, CO, and OH according to the contributions of each injection of a split-injection diesel jet. Fuel and CO are at the start of second-stage ignition, and the OH is after the peak heat-release rate.

Conclusions

- Cylinder-wall heat flux measurements coupled with simultaneous OH* chemiluminescence imaging provide phenomenological insight into in-cylinder physical and chemical processes affecting heat transfer losses.
- Heat flux increases ahead of jet impingement for both CDC and LTC, which is consistent with hypothesis of boundary layer compression by penetrating jet, but further experiments are required to confirm the hypothesis.
- Future data analysis will provide similar insight into heat losses across multiple combustion modes.
- Split-injection simulations predict little displacement of the 1st-injection residual jet by the 2nd injection, but much inter-jet mixing. Ignition products are from the 1st-injection fuel, but no ignition occurs without the 2nd injection. These predictions help to guide experiments.

Key Publications/Presentations

1. "Isolating the effects of reactivity stratification in reactivity-controlled compression ignition with iso-octane and n-heptane on a light-duty multi-cylinder engine," Wissink ML, Curran SJ, Roberts G, Musculus MPB, Mounaïm-Rousselle C, Int. J. Engine Research 19(9):907-926 (November 2018)
2. "A visual investigation of CFD-predicted in-cylinder mechanisms that control first- and second-stage ignition in diesel jets," Hessel R, Reitz R, Musculus MPB, SAE Technical Paper 2019-01-0543 (April 2019)
3. "Dilution and injection pressure effects on ignition and onset of soot at threshold-sooting conditions by simultaneous PAH-PLIF and soot-PLII imaging in a heavy duty optical diesel engine," Li Z, Roberts G, Musculus MPB, SAE Technical Paper 2019-01-0553 (April 2019)
4. "Investigation of fuel condensation processes under non-reacting conditions in an optically-accessible engine," Qiu L, Reitz R, Eagle E, Musculus MPB, SAE Technical Paper 2019-01-0197 (2019)

5. “Multiple injection interactions on ignition and onset of soot by simultaneous PAH-PLIF and soot-PLII imaging,” Li Z, Musculus M, AEC Meeting, USCAR, Southfield MI (August 2018)
6. “How jets get it all mixed up: Combustion research using laser diagnostics in optical engines at Sandia National Laboratories,” Musculus M, Technical Seminar, UC Davis (November 2018)
7. “Experimental investigation of cylinder-wall heat flux under five combustion modes: CDC, SIDI, HCCI, PPCI, RCCI,” Li Z, Musculus M, AEC Meeting, ORNL (January 2019)
8. “Comparison of combustion modes,” Musculus M, Co-Optima 4th Annual All Hands Meeting, ORNL (March 2019)
9. “The benefits and challenges of pushing engine BTE to very high levels (60%+): where is the point of diminishing returns?,” Musculus M, Splitter D, Kelly K, Zhang C, Miles P, Wagner R, 21st Century Truck Partnership IC Powertrain Tech Team Meeting videoconference (April 2019)

References

1. Splitter DA, Hanson RM, Kokjohn SL, Reitz RD “Reactivity controlled compression ignition (RCCI) heavy-duty engine operation at mid-and high-loads with conventional and alternative fuels,” SAE Technical Paper 2011-01-0363 (2011)
2. Mohr D, Shipp T, Lu X, “The thermodynamic design, analysis and test of Cummins’ Supertruck 2 50% brake thermal efficiency engine system,” SAE Technical Paper 2019-01-0247 (2019)
3. Pickett L, López J, “Jet-wall interaction effects on diesel combustion and soot formation,” SAE Technical Paper 2005-01-0921 (2005)

Acknowledgements

This research was sponsored by the U.S. Department of Energy (DOE) Office of Energy Efficiency and Renewable Energy (EERE). Optical engine experiments were conducted at the Combustion Research Facility, Sandia National Laboratories, Livermore, CA. Sandia National Laboratories is a multi-mission laboratory managed and operated by National Technology and Engineering Solutions of Sandia, LLC., a wholly owned subsidiary of Honeywell International, Inc., for the U.S. Department of Energy’s National Nuclear Security Administration under contract DE-NA0003525.

Acronyms, Abbreviations, Symbols, and Units

AHRR Apparent Heat Release Rate
CAD Crank Angle Degrees (360 = TDC compression)
CDC Conventional Diesel Combustion
CO Carbon Monoxide
EGR Exhaust Gas Recirculation
FY Fiscal Year
GDI Gasoline Direct Injection
HCCI Homogeneous-Charge Compression Ignition
HF Heat Flux
HT Heat Transfer
ICMOS Intensified Complementary Metal Oxide Semiconductor camera
IMEPg Indicated Mean Effective Pressure (gross)
LTC Low-Temperature Combustion
LTHR Low-Temperature Heat Release
OH Hydroxyl radical
OH* Excited-state hydroxyl radical
PPCI Partially Premixed Compression Ignition
PRF Primary Reference Fuel
RCCI Reactivity-Controlled Compression Ignition
SNL Sandia National Laboratories
WERC Wisconsin Engine Research Consultants